

Electrodeposition of Lead from 1-Methylimidazolium Trifluoromethylsulfonate Ionic Liquid

Min Li^{1,2,*}, Ying Li^{1,2,*}

¹ School of Metallurgy, Northeastern University, Shenyang 110819, China

² Liaoning Key Laboratory for Metallurgical Sensor and Technology, Northeastern University, Shenyang 110819, China

*E-mail: lim@smm.neu.edu.cn, gaoanlimin@163.com; liying@mail.neu.edu.cn

Received: 7 June 2018 / Accepted: 25 July 2018 / Published: 1 September 2018

In this work, it found that lead oxide (PbO) can be dissolved well in 1-methylimidazolium trifluoromethylsulfonate (MIMTfO) ionic liquid. The electrodeposition of lead from PbO in MIMTfO ionic liquid was studied. Cyclic voltammetry studies showed that the reduction of Pb(II) is a irreversible and one-step reaction process. Chronoamperometry results presented that the nucleation mechanism of lead is fit instantaneous nucleation under diffusion control. The diffusion coefficient of Pb(II) at 373 K is approximately $3.6 \times 10^{-8} \text{ cm}^2 \text{ s}^{-1}$. The electrodeposition experiments were conducted at 383 K and 393 K using potentiostatic electrolysis. A compact electrodeposit was obtained at 383 K in MIMTfO ionic liquid, which was confirmed to be metallic lead.

Keywords: lead; electrodeposition; ionic liquid; cyclic voltammetry; chronoamperometry

1. INTRODUCTION

Lead is a very important metal because of its unique properties and has been widely used in various fields, such as lead-acid batteries, electrochromic devices, and semiconductors [1–4]. Lead is also the suitable material for exploring oil and gas, protecting radiological medical, shielding industrial X-ray, and so on [5,6]. The electrodeposition of lead at low temperature are mainly studied in aqueous solutions [7–15]. However, the electrodeposition process often involves hydrogen evolution and harmful chemicals (such as corrosive acids and cyanides). To overcome the shortcomings, researchers have transferred their attention to ionic liquids, which are considered as excellent media for electrodeposition of metals since they usually exhibit very low vapor pressure, excellent conductivity and thermal stability, and large electrochemical windows [16,17].

The electrodeposition of lead has been reported in several ionic liquids. Hussey et al. [18]

reported the electroreduction of Pb(II) in the AlCl₃-1-methyl-3-ethylimidazolium chloride (66.7-33.3 mol%) using a glassy carbon electrode at 313 K. It found that the electrodisolution of lead was a quasi-reversible reaction, while the reduction of Pb(II) on the glassy carbon electrode exhibited progressive nucleation process. The diffusion coefficient of Pb(II) was $9.0 \times 10^{-7} \text{ cm}^2 \text{ s}^{-1}$. Katayama et al. [19] showed the electroreduction of Pb(II) in 1-butyl-1-methylpyrrolidinium bis(trifluoromethylsulfonyl)amide (BMPTFSA) ionic liquid with Pb(TFSA)₂ as the Pb(II) source. Cyclic voltammetry result indicated that the onset electroreduction potential of lead was -0.68 V (vs. Ag/Ag⁺). Chronoamperometry result revealed that the diffusion coefficient of Pb(II) at 298 K was $8.0 \times 10^{-8} \text{ cm}^2 \text{ s}^{-1}$. The calculated diffusion coefficient was in good agreement with those of divalent metal species in BMPTFSA ionic liquid. Additionally, it found that the nucleation mechanism and the surface morphology of electrodeposits strongly depended on the deposition potential. Sun et al. [20] studied the voltammetric curve of Pb(II) in 1-ethyl-3-methylimidazolium tetrafluoroborate ionic liquid. The electrodeposition of lead was performed on a nickel electrode using constant applied potential. The nucleation mechanism of lead was much more likely to fit instantaneous nucleation under diffusion control. MacFarlane et al. [21] researched the electrochemical behavior and electrodeposition morphology of Pb(II) in 1-ethyl-3-methylimidazolium bis(trifluoromethylsulfonyl)amide ionic liquid. Cyclic voltammetry experiments presented that the electrochemical behavior of Pb(II) depended on the applied working electrode material. The platinum and lead electrodes exhibited the highest current and lowest overpotential for the electrodeposition process. Chronoamperometric analysis suggested that the electrodeposition of lead at all the applied substrate followed a three-dimensional progressive nucleation process. However, the surface morphology of the lead coatings was mainly affected by the electrodeposition substrate. Chen et al. [22] found that PbO and PbO₂ can be dissolved in protonated betaine bis(trifluoromethylsulfonyl)amide ([Hbet][TFSA]) ionic liquid. The uniform lead coatings were successfully electrodeposited using potentiostatic and galvanostatic techniques. It also found that the morphologies of lead electrodeposits obtained from [Hbet][TFSA] ionic liquid and deep eutectic solvents were dissimilar, which may be due to the formation of different lead species in the electrolytes. Besides the above mentioned ionic liquids, the electrodeposition of lead from lead oxide has been mainly studied in deep eutectic solvents [23–29]. Although the electrodeposition of lead has been studied in several kinds of electrolytes, the investigation of electroreduction and nucleation mechanisms of lead from PbO in MIMTfO ionic liquid has not been found.

In this work, the electrochemical behavior and electrodeposition of lead from PbO in MIMTfO ionic liquid was reported. SEM-EDS and XRD methods were used to detect the obtained electrodeposits.

2. EXPERIMENTAL

The MIMTfO ionic liquid (Shanghai Cheng Jie Chemical Co., Ltd, China, 98%) and PbO (Aladdin, 99.9%) were used as received. The MIMTfO ionic liquid was melted at 373 K under a argon atmosphere, and then PbO was added to the ionic liquid followed by stirring for few minutes until a clear and colorless solution was obtained.

Cyclic voltammetry and chronoamperometry were achieved under a argon atmosphere using a CHI 660E Electrochemical System (Shanghai Chenhua, China). The scan rate of the cyclic voltammetry studies was 50 mV s^{-1} without mentioned. A tungsten wire (Alfa Aesar, $\geq 99.95\%$, 0.157 cm^2), a platinum wire (Alfa Aesar, $\geq 99.99\%$), and a silver wire (Alfa Aesar, 99.9%) were used as the working electrode, the counter electrode, and the quasi-reference electrode. All the electrodes were polished successively with increasingly finer grades of emery paper, cleaned with anhydrous ethanol, rinsed with distilled water, and finally air dried before measurements. The electrodeposition experiments were performed on a copper plate (Alfa Aesar, 99.9% , 0.25 cm^2) under a argon atmosphere using potentiostatic electrolysis. The lead electrodeposits were cleaned with anhydrous ethanol to remove residual ionic liquids. A high-resolution scanning electron microscope (SEM, Shimadzu SSX-550, Japan) attached with energy dispersive spectroscope (EDS) working at 15 kV was utilized to study the surface morphologies and compositions of the lead electrodeposits. A X-ray diffraction (XRD, PANalytical MPDDY 2094, Netherlands) using $\text{Cu K}\alpha$ line working at 40 kV and 40 mA was used to determine the phases and structures of the samples.

3. RESULTS AND DISCUSSION

3.1. Cyclic voltammetry

The electrochemical window of MIMTfO ionic liquid was firstly studied at 373 K using cyclic voltammetry (CV) (Fig. 1). Cyclic voltammogram shows that the cathodic and anodic limits for MIMTfO ionic liquid are -1.0 V and 3.5 V (vs. Ag), respectively. Therefore, the electrochemical window of MIMTfO ionic liquid at 373 K is found to be approximately 4.5 V . In addition, no obvious current is observed within the electrochemical window range, indicating that the MIMTfO ionic liquid is in a high purity.

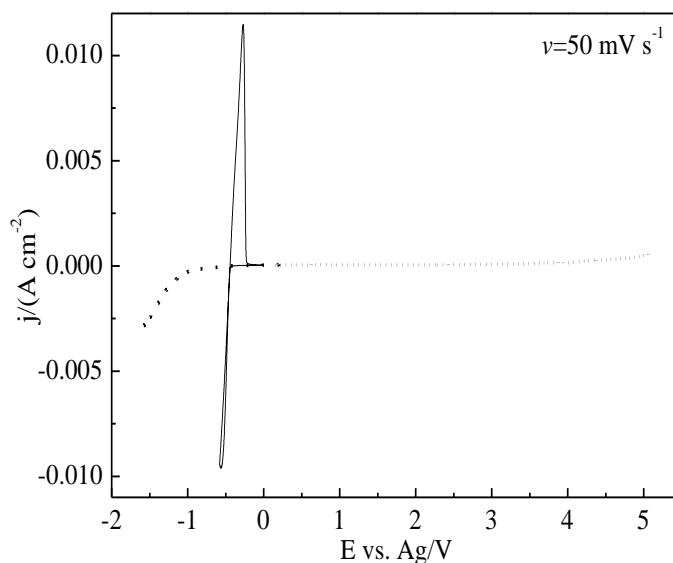


Figure 1. Cyclic voltammograms of MIMTfO ionic liquid without (dotted) and with (solid) 0.15 mol L^{-1} PbO recorded on a tungsten electrode at 373 K . The scan rate was 50 mV s^{-1} .

Then CV was performed in MIMTfO ionic liquid containing 0.15 mol L^{-1} PbO to investigate the electrochemical behavior of Pb(II). As shown in Fig. 1, a reduction wave with peak potential at approximately -0.55 V (vs. Ag) and a oxidation wave with peak potential at approximately -0.27 V (vs. Ag) are observed in MIMTfO ionic liquid with the addition of Pb(II). It should be noted that the reduction and oxidation waves only appeared in the presence of Pb(II) ions. Meantime, the electrodeposit obtained in the reduction current peak potential region was further confirmed as metallic lead. Thus, the reduction and oxidation peaks corresponding to the electrodeposition and stripping of lead. The identical cathodic reaction ($\text{Pb(II)} + 2\text{e}^- \rightarrow \text{Pb}$) has been reported in literature regardless of the Pb(II) sources are oxide or not [18–22,24–29]. In addition, a classic crossover current loop is found, which suggests that a nucleation process exists in the electroreduction of Pb(II). The similar nucleation phenomenon for electrodeposition of lead has also been found by many researchers [18–21,27,29].

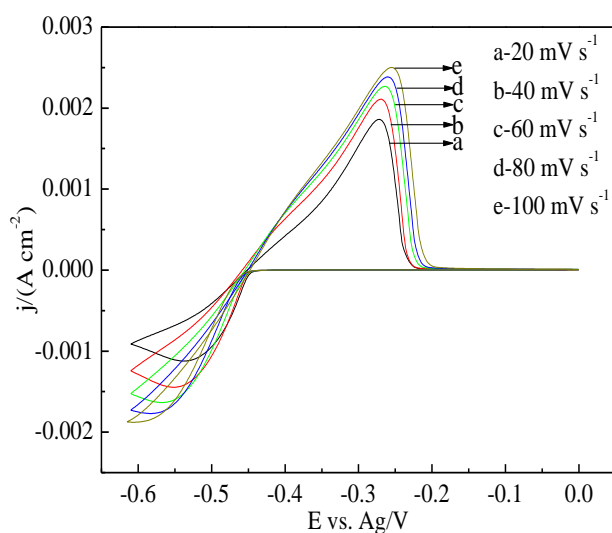


Figure 2. Cyclic voltammograms of MIMTfO ionic liquid containing 0.15 mol L^{-1} PbO recorded on a tungsten electrode at 373 K under different scan rates.

Fig. 2 presents the cyclic voltammograms of MIMTfO ionic liquid with PbO as Pb(II) source recorded at 373 K under different scan rates. It can be seen that the reduction current peak potentials shift toward more negative potential with the increasing of the scan rate and the difference of potential (more than 850 mV) between the reduction and oxidation peaks is much more larger than the theoretical value expected for a reversible reaction, indicating that the electrode reaction of Pb(II) to Pb is irreversible. The similar behavior was also observed for the CV of Pb [20,24,29], La [30], Ni [31–33], and Co [34,35] in ionic liquids. Based on the analysis of Figs. 1 and 2, it can conclude that the electrodeposition of lead in MIMTfO ionic liquid is a irreversible, single-step, and two-electrons reaction process.

3.2. Chronoamperometry

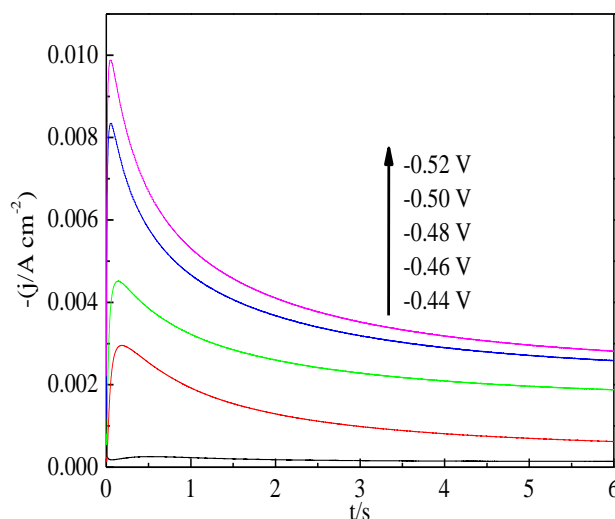


Figure 3. Current density-time transients of chronoamperometric experiments for MIMTfO ionic liquid containing 0.15 mol L^{-1} PbO recorded on a tungsten electrode at 373 K.

As mentioned in Fig. 1, a nucleation process exists in the electroreduction of Pb(II). Chronoamperometry was performed at 373 K to further determine the nucleation mechanism of lead in MIMTfO ionic liquid. It was performed by starting the potential of the working electrode from a value at which no Pb(II) electroreduction occurred to a value where sufficiently negative to initiate the nucleation and growth process. Fig. 3 presents the obtained current-time transient curves. It can be seen that all these transient curves display the typical behavior of a nucleation process [18–21,24,29,31,33,35,38,39]: after the decay of a sharp electrode double-layer charging current, an increase in the faradaic current was observed due to the nucleation and growth of Pb nuclei. The cathodic current reaches a peak current maximum, i_m , as the discrete diffusion zones of individual growing crystallites begin to overlap at time t_m . All the current transients decay slowly after t_m because of the increase in the diffusion layer thickness. i_m increases and t_m decreases with increasing the applied cathodic potential. The currents decay linearly with $t^{-1/2}$, which is consistent with the Cottrell equation [36]:

$$I = nFAD^{1/2}C(\pi t)^{-1/2} \quad (1)$$

where I is the current passing through electrolyte in A, n is the number of transferred electrons, F is the Faraday constant, 96485 C mol^{-1} , A is the electrode area in cm^2 , D is the diffusion coefficient of electro-active species in $\text{cm}^2 \text{ s}^{-1}$, C is the bulk concentration in mol cm^{-3} , and t is the time in s. The plots of current density (j) vs. time ($t^{-1/2}$) for four potentials almost give a straight line (Fig. 4) similar to the result reported in references [24,33]. Using Eq. (1) and the obtained slopes, the diffusion coefficient of Pb(II) in MIMTfO ionic liquid for different potentials can be obtained, as presented in Table 1. Therefore, the average value of the diffusion coefficient for Pb(II) at 373 K was calculated to be $3.6 \times 10^{-8} \text{ cm}^2 \text{ s}^{-1}$.

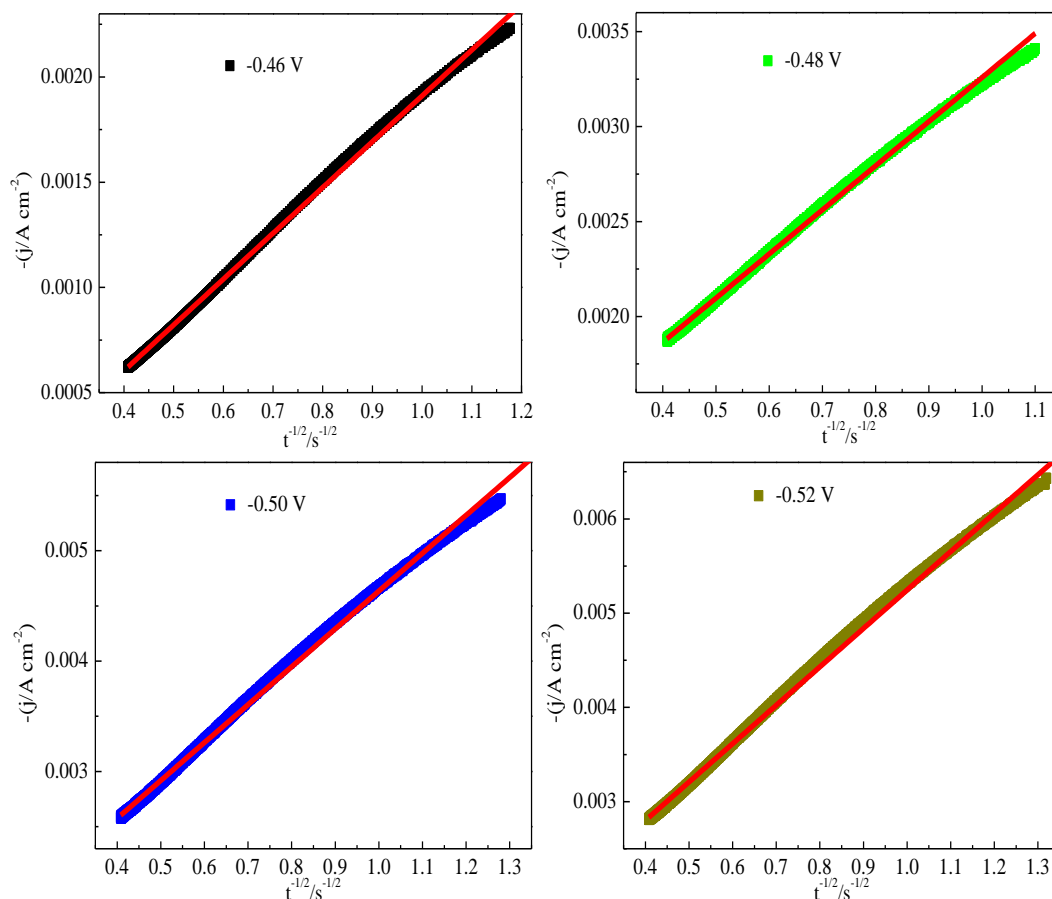


Figure 4. Variation of current density (j) with time ($t^{-1/2}$) for the decreasing portions of the current density-time transients in Figure 3 during the electrodeposition of lead on a tungsten electrode at 373 K.

Table 1. The diffusion coefficient of Pb(II) calculated from the Cottrell equation at different potentials.

| Potential (V) | D ($\text{cm}^2 \text{s}^{-1}$) |
|---------------|-------------------------------------|
| -0.46 | 1.8×10^{-8} |
| -0.48 | 2.0×10^{-8} |
| -0.50 | 4.4×10^{-8} |
| -0.52 | 6.2×10^{-8} |
| Average | 3.6×10^{-8} |

Table 2. Comparison of the diffusion coefficient of Pb(II) in various ionic liquids.

| Authors | System | Temperature (K) | D ($\text{cm}^2 \text{s}^{-1}$) |
|------------------------|--|-----------------|-------------------------------------|
| Hussey et al. [18] | PbCl ₂ in AlCl ₃ -EMIC | 313 | 9.0×10^{-7} |
| Katayama et al. [19] | Co(TFSA) ₂ in BMPTFSA | 298 | 8.0×10^{-8} |
| MacFarlane et al. [21] | Pb(TFSA) ₂ in EMIMTFSA | 293 | 1.3×10^{-7} |
| Reddy et al. [24] | PbO in urea-choline chloride | 363 | 2.4×10^{-7} |
| Sun et al. [29] | PbO in urea-choline chloride | 363 | 2.2×10^{-7} |
| Sun et al. [29] | PbO ₂ in urea-choline chloride | 363 | 9.1×10^{-8} |

| | | | |
|-------------------|--|-----|----------------------|
| Sun et al. [29] | PbSO ₄ in urea-choline chloride | 363 | 8.6×10 ⁻⁸ |
| Bhatt et al. [37] | Pb(NO ₃) ₂ in DIMCARB | 298 | 1.4×10 ⁻⁷ |
| This work | PbO in MIMTfO | 373 | 3.6×10 ⁻⁸ |

A summary of chronoamperometry studies on diffusion coefficient of Pb(II) ions in various ionic liquids is given in Table 2. It shows that the diffusion coefficient values for Pb(II) ions are generally in the range of 10⁻⁷ to 10⁻⁸ with different applied temperatures, Pb(II) sources, and ionic liquids, which may be mainly due to different physicochemical properties of used ionic liquids and different electro-active species formed in ionic liquids.

According to the Scharifker-Hills nucleation model, the nucleation mechanism can be classified as either instantaneous (Eq. (2)) or progressive (Eq. (3)). The instantaneous model refers to that all nucleation sites are activated at the same time after the potential step, while the progressive model refers to that the nucleation sites are gradually activated when the potential is applied [38,39]. The two nucleation mechanism can be distinguished by comparing the experimental data to the theoretical dimensionless $(i/i_m)^2$ vs (t/t_m) curves.

$$\left(\frac{i}{i_m}\right)^2 = 1.9542\left(\frac{t_m}{t}\right)\left(1 - \exp\left[-1.2564\left(\frac{t}{t_m}\right)\right]\right)^2 \quad (2)$$

$$\left(\frac{i}{i_m}\right)^2 = 1.2254\left(\frac{t_m}{t}\right)\left(1 - \exp\left[-2.3367\left(\frac{t}{t_m}\right)^2\right]\right)^2 \quad (3)$$

Based on the above mentioned treatment, the normalized experimental and theoretical plots were depicted. As shown in Fig. 5, it can be seen that the reduction of Pb(II) on the tungsten electrode is much more likely to fit instantaneous nucleation with diffusion control. A similar instantaneous nucleation mechanism for lead electrodeposition has also been reported in BMPTFSA [19] and EMIMBF₄ [20] ionic liquid, and deep eutectic solvents [24,29].

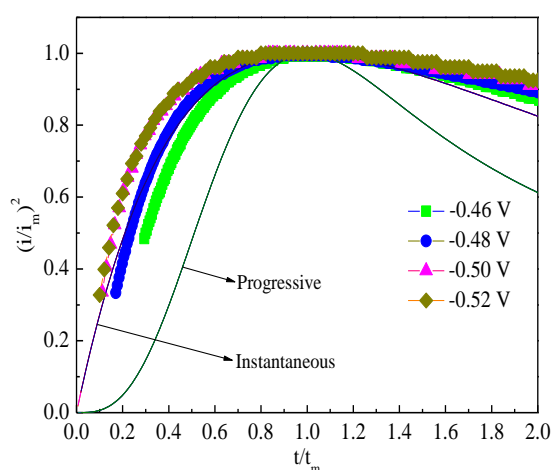


Figure 5. Comparison between theoretical and experimental $(i/i_m)^2$ vs. (t/t_m) plot for lead electrodeposition on a tungsten electrode at different potentials.

However, the electrodeposition of lead involved the progressive nucleation mechanism was observed in $\text{AlCl}_3\text{-EMIC}$ [18], EMIMTfSA [21], and DIMCARB (a mixture of adducts of dimethylamine and carbon dioxide) [37] ionic liquids, indicating that the type of ionic liquids may have an effect on the nucleation mechanism.

Once the nucleation process was determined to be instantaneous, the diffusion coefficient of Pb(II) can also be determined using the following equation [38,39]:

$$j_m^2 t_m = 0.1629(nFC)^2 D \quad (4)$$

where j_m is the maximum current density in A cm^{-2} . Using Eq. (4) and the values of j_m and t_m obtained from the current density-time transients, the diffusion coefficient of Pb(II) in MIMTfO ionic liquid for different potentials can be obtained (Table 3), and the average value of the diffusion coefficient for Pb(II) was calculated to be $2.8 \times 10^{-8} \text{ cm}^2 \text{ s}^{-1}$, which is close to the value ($3.6 \times 10^{-8} \text{ cm}^2 \text{ s}^{-1}$) calculated from the Cottrell equation.

Table 3. The diffusion coefficient of Pb(II) calculated from the maximum of current density-time transients at different potentials.

| Potential (V) | $D (\text{cm}^2 \text{ s}^{-1})$ |
|---------------|----------------------------------|
| -0.46 | 1.4×10^{-8} |
| -0.48 | 2.2×10^{-8} |
| -0.50 | 3.3×10^{-8} |
| -0.52 | 4.4×10^{-8} |
| Average | 2.8×10^{-8} |

In addition, the number density of nucleation (N) can be determined using the following Eqs. (5) and (6) [38,39]:

$$j_m = 0.6382nFCD(kN)^{1/2} \quad (5)$$

$$k = (8\pi CM/\rho)^{1/2} \quad (6)$$

where N is the number density of nucleation in cm^{-2} , k is a numerical constant determined by the experimental conditions, M and ρ are the molecular weight (207.2 g mol^{-1}) and density (11.3 g cm^{-3}) of the deposited material, lead, respectively. Using Eq. (5) and the values of j_m and k , the number density of nucleation for Pb(II) can be obtained, as presented in Table 4.

Table 4. The number density of nucleation for Pb(II) at different potentials.

| Potential (V) | $N (\text{cm}^{-2})$ |
|---------------|----------------------|
| -0.46 | 1.2×10^8 |
| -0.48 | 2.9×10^8 |
| -0.50 | 9.9×10^8 |
| -0.52 | 1.4×10^9 |

It can be seen that the number density of nucleation for Pb(II) lies between $1.2 \times 10^8 \text{ cm}^{-2}$ and $1.4 \times 10^9 \text{ cm}^{-2}$ at 373 K and it increases with the increasing of the applied cathodic potential.

3.3. Electrodeposition and characterization of lead

Fig. 6 presents the SEM micrographs of the lead coatings electrodeposited at -0.50 V in MIMTfO ionic liquid containing $0.15 \text{ mol L}^{-1} \text{ PbO}$ at 383 K and 393 K. It shows that a uniform and compact electrodeposit is observed at 383 K (Fig. 6a), while a dendritic electrodeposit is observed as the temperature increased to 393 K (Fig. 6b), which may be mainly due to the different deposition rate at different temperature. The chemical composition of the obtained coating was also analyzed using EDS spectrum.

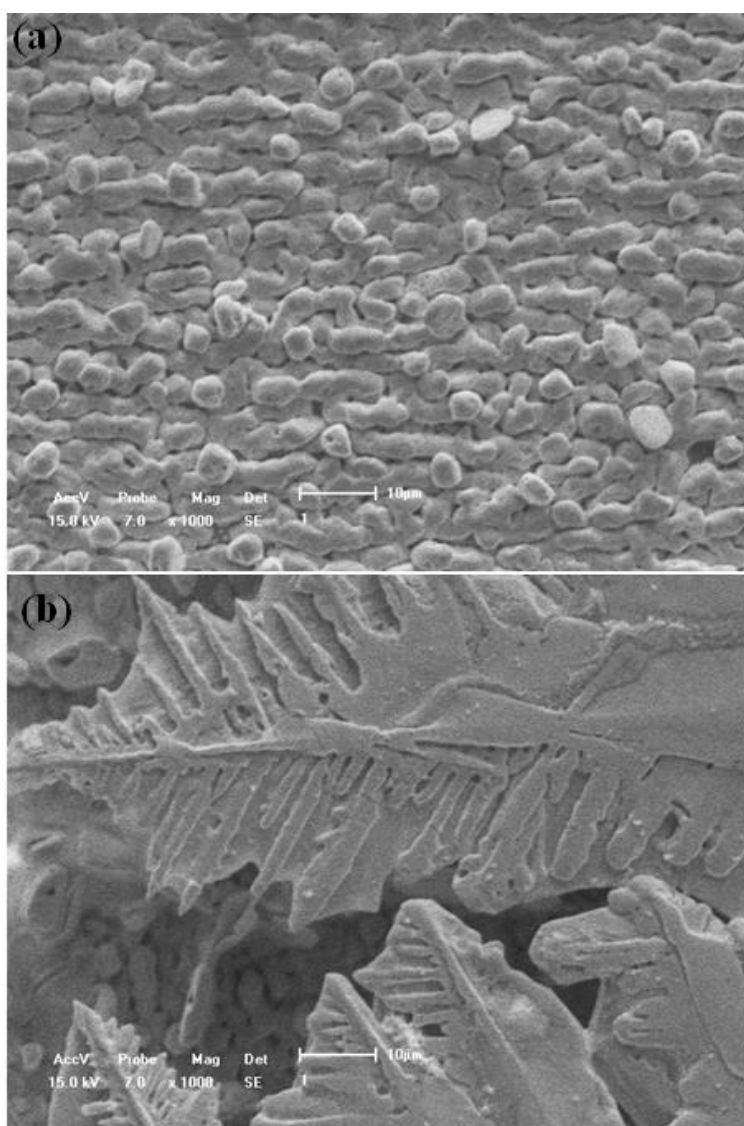


Figure 6. SEM micrographs of lead electrodeposits obtained from MIMTfO ionic liquid containing $0.15 \text{ mol L}^{-1} \text{ PbO}$ at -0.50 V on a copper substrate at different temperatures: (a) 383 K, and (b) 393 K.

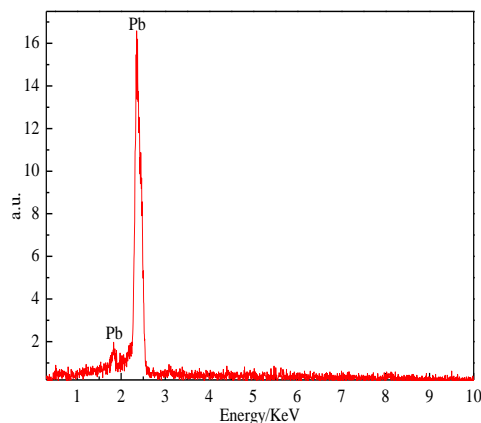


Figure 7. EDS spectrum of the lead electrodeposit obtained from MIMTfO ionic liquid containing 0.15 mol L^{-1} PbO on a copper substrate at -0.50 V and at 383 K .

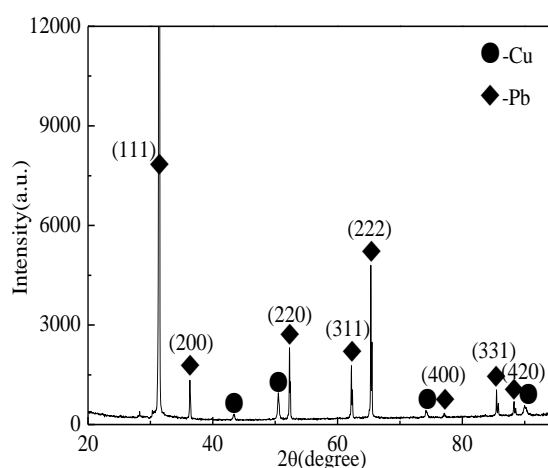


Figure 8. XRD pattern of the lead electrodeposit obtained from MIMTfO ionic liquid containing 0.15 mol L^{-1} PbO on a copper substrate at -0.50 V and at 383 K .

As shown in Fig. 7, it only exhibits the strong peaks of lead, indicating that the main chemical composition of the obtained electrodeposit is lead. Moreover, it is not found any obvious impurity peaks, which indicates that the obtained electrodeposit is free of residual ionic liquid.

The crystalline structure of the obtained electrodeposit was investigated using XRD (Fig. 8). It can be seen that all the marked peaks in the pattern can be assigned to metallic lead except the peaks of the copper substrate. Meantime, the obtained lead electrodeposit exhibits eight diffraction peaks (111), (200), (220), (311), (222), (400), (331), (420), and the diffraction peak of (111) is the strongest, indicating that a favorable orientation was formed. The identical favorable orientation was also observed for lead electrodeposition obtained in EMIMBF₄ [20], EMIMTfSA [21], and DIMCARB [37] ionic liquids.

4. CONCLUSIONS

The MIMTfO ionic liquid can dissolve PbO very well and was used as the electrolyte to study

the electrodeposition of lead at 373 K in this work. Cyclic voltammetry studies showed that the reduction and oxidation peaks corresponding to the electrodeposition and stripping of lead are observed. Chronoamperometry results revealed that the electroreduction of Pb(II) on the working electrode is much more likely to fit instantaneous nucleation. Calculated from the Cottrell equation, the diffusion coefficient of Pb(II) was found to be approximately $3.6 \times 10^{-8} \text{ cm}^2 \text{ s}^{-1}$ at 373 K, which is close to the value ($2.8 \times 10^{-8} \text{ cm}^2 \text{ s}^{-1}$) obtained from the maximum of current density-time curves. Additionally, the number density of nucleation for Pb(II) was obtained and it increases with the increasing of the applied cathodic potential. A compact lead electrodeposit was achieved at lower temperature, which was confirmed to be metallic lead by EDS and XRD.

ACKNOWLEDGEMENTS

The authors would like to express their gratitude for the financial support provided by the Fundamental Research Funds for the Central Universities (Grant Nos. N172503018, N162410002-15, N172507011, N172506010), the China Postdoctoral Science Foundation (Grant No. 2018M630298) and Postdoctoral Science Foundation from Northeastern University of China (Grant No. 20180202), and the National Natural Science Foundation of China (Grant Nos. 51774076, 51474057).

References

1. D. Pavlov, *J. Power Sources*, 42 (1993) 345.
2. B. Rashkova, B. Guel, R.T. Potzschke, G. Staikov and W.J. Lorenz, *Electrochim. Acta*, 43 (1998) 3021.
3. C. Ehlers, U. Konig, G. Staikov and J.W. Schultze, *Electrochim. Acta*, 47 (2001) 379.
4. C.O. Avellaneda, M.A. Napolitano, E.K. Kaibara and L.O.S. Bulhoes, *Electrochim. Acta*, 50 (2005) 1317.
5. N.D. Nikolic, G. Brankovic and U.C. Laenjevac, *J. Solid State Electrochem.*, 16 (2012) 2121.
6. N.D. Nikolic, K.I. Popov, P.M. Zivkovic and G. Brankovic, *J. Electroanal. Chem.*, 691 (2013) 66.
7. J. Mostany, J. Parra and B.R. Scharifker, *J. Appl. Electrochem.*, 16 (1986) 333.
8. L. Muresan and L. Oniciu, *J. Appl. Electrochem.*, 23 (1993) 66.
9. L. Muresan and L. Oniciu, *J. Appl. Electrochem.*, 24 (1994) 332.
10. K.I. Popov, E.R. Stojilkovic, V. Radmilovic and M.G. Pavlovic, *Powder Technol.*, 93 (1997) 55.
11. E. Exposito, J.G.-Garcia, P. Bonete, V. Montiel and A. Aldaz, *J. Power Sources*, 87 (2000) 137.
12. L. Doulakas, K. Novy, S. Stucki and C. Comninellis, *Electrochim. Acta*, 46 (2000) 349.
13. I.A. Carlos, M.A. Malaquias, M.M. Oizumi and T.T. Matsuo, *J. Power Sources*, 92 (2001) 56.
14. S.M. Wong and L.M. Abrantes, *Electrochim. Acta*, 51 (2005) 619.
15. M.F. Cabral, M.L. Calegario and S.A.S. Machado, *RSC Adv.*, 2 (2012) 2498.
16. A.P. Abbott, K.S. Ryder and U. Konig, *Trans. Inst. Met. Finish*, 86 (2008) 196.
17. S.Z.E. Abedin and F. Endres, *ChemPhysChem*, 7 (2006) 58.
18. C.L. Hussey and X.H. Xu, *J. Electrochem. Soc.*, 138 (1991) 1886.
19. Y. Katayama, R. Fukui and T. Miura, *J. Electrochem. Soc.*, 160 (2013) D251.
20. R.-W. Tsai, Y.-T. Hsieh, P.-Y. Chen and I.-W. Sun, *Electrochim. Acta*, 137 (2014) 49.
21. T.J. Simons, A.K. Pearson, S.J. Pas and D.R. MacFarlane, *Electrochim. Acta*, 174 (2015) 712.
22. H.-W. Yeh, Y.-H. Tang and P.-Y. Chen, *J. Electroanal. Chem.*, 811 (2018) 68.
23. A.P. Abbott, G. Capper, D.L. Davies, K.J. Mckenzie and S.U. Obi, *J. Chem. Eng. Data*, 51 (2006) 1280.
24. H.X. Yang and R.G. Reddy, *J. Electrochem. Soc.*, 161 (2014) D586.
25. A. Bakkar, *J. Hazard. Mater.*, 280 (2014) 191.
26. J.J. Ru, Y.X. Hua, C.Y. Xu, J. Li, Y. Li, D. Wang, C.C. Qi and Y.F. Jie, *Appl. Surf. Sci.*, 335

- (2015) 153.
27. J.J. Ru, Y.X. Hua, C.Y. Xu, J. Li, Y. Li, D. Wang, K. Gong and Z.R. Zhou, *Adv. Powder Technol.*, 26 (2015) 91.
 28. J.J. Ru, Y.X. Hua, D. Wang, C.Y. Xu, J. Li, Y. Li, Z.R. Zhou and K. Gong, *Electrochim. Acta*, 186 (2015) 455.
 29. Y.-S. Liao, P.-Y. Chen and I-W. Sun, *Electrochim. Acta*, 214 (2016) 265.
 30. Q.B. Zhang, C. Yang, Y.X. Hua, Y. Li and P. Dong, *Phys. Chem. Chem. Phys.*, 17 (2015) 4701.
 31. Y.-L. Zhu, Y. Kozuma, Y. Katayama and T. Miura, *Electrochim. Acta*, 54 (2009) 7502.
 32. M. Li, Z.W. Wang and R.G. Reddy, *J. Electrochem. Soc.*, 161 (2014) D150.
 33. M. Li, B.L. Gao, Z.N. Shi, X.W. Hu, S.X. Wang, L.X. Li, Z.W. Wang and J.Y. Yu, *Electrochim. Acta*, 169 (2015) 82.
 34. M. Li, Z.W. Wang and R.G. Reddy, *Electrochim. Acta*, 123 (2014) 325.
 35. M. Li, B.L. Gao, Z.N. Shi, X.W. Hu, S.X. Wang, L.X. Li, Z.W. Wang and J.Y. Yu, *J. Solid State Electrochem.*, 20 (2016) 247.
 36. A.J. Bard and R.L. Faulkner, *Electrochemical methods fundamentals and applications*, John Wiley & Sons, (2001) New York, USA.
 37. A.I. Bhatt, A.M. Bond and J. Zhang, *J. Solid State Electrochem.*, 11 (2007) 1593.
 38. G. Gunawardena, G. Hills, I. Montenegro and B. Scharifker, *J. Electroanal. Chem.*, 138 (1982) 225.
 39. B. Scharifker and G. Hills, *Electrochim. Acta*, 28 (1983) 879.

© 2018 The Authors. Published by ESG (www.electrochemsci.org). This article is an open access article distributed under the terms and conditions of the Creative Commons Attribution license (<http://creativecommons.org/licenses/by/4.0/>).